Mathematical model with spatially uniform regulation explains long-range bidirectional transport of early endosomes in fungal hyphae

Jia Gou[a], Leah Edelstein-Keshet[a], and Jun Allard[b]
[a]Department of Mathematics, University of British Columbia, Vancouver, BC V6T1Z2, Canada; [b]Department of Mathematics, Department of Physics and Astronomy, and Center for Complex Biological Systems, University of California, Irvine, Irvine, CA 92617

ABSTRACT In many cellular contexts, cargo is transported bidirectionally along microtubule bundles by dynein and kinesin-family motors. Upstream factors influence how individual cargoes are locally regulated, as well as how long-range transport is regulated at the whole-cell scale. Although the details of local, single-cargo bidirectional switching have been extensively studied, it remains to be elucidated how this results in cell-scale spatial organization. Here we develop a mathematical model of early endosome transport in *Ustilago maydis*. We demonstrate that spatiotemporally uniform regulation, with constant transition rates, results in cargo dynamics that is consistent with experimental data, including data from motor mutants. We find that microtubule arrays can be symmetric in plus-end distribution but asymmetric in binding-site distribution in a manner that affects cargo dynamics and that cargo can travel past microtubule ends in microtubule bundles. Our model makes several testable predictions, including secondary features of dynein and cargo distributions.

INTRODUCTION

Long-range transport of material is an essential process in cells of the CNS, whose length can span ≥1 m. Even in the shortest neurons, with lengths on the order of tens or hundreds of micrometers, the transport of vesicles from cell body to synapses at cell ends has proven a challenging process to understand. Partly for this reason, model organisms in which related processes take place have led to insights about the underlying phenomena. These include the assembly and disassembly of microtubules (MTs), their dynamic stability properties, the roles of motors such as kinesin and dynein that move along these asymmetric tracks, and the competition of these molecular motors for the cargo that they transport. The presence of multiple interacting components and their collective behaviors make these systems ripe for mathematical modeling (Bressloff and Newby, 2013), which can integrate observations of multiple components into a unified, coherent framework.

Much recent work has focused on the molecular nature of bidirectional motor transport of cargo along MTs (Shubeita and Gross, 2012) and whether reversal of direction arises from upstream regulation (Kunwar *et al.*, 2011; Leidel *et al.*, 2012) or a spontaneous stochastic "tug-of-war" between competing families of motors (Muller *et al.*, 2008; Soppina *et al.*, 2009; Hendricks *et al.*, 2012a). However, regardless of local molecular mechanism, there remains an important systems-level question: at the cell scale, is cargo transport self-organized, or does it require spatiotemporally organized regulation? Specifically, can the observed dynamics be entirely explained by local concentrations of motors, MTs, and cargo, with rate constants that are uniform in space and time (suggesting self-organization), or must these rate constants be spatially nonuniform (suggesting organization by upstream spatiotemporal regulation)? Cytoskeletal assembly and actin dynamics in cell polarization and chemotaxis are spatially regulated by signaling proteins such as Rho-family GTPAses (Ridley and Hall, 1992; Hall, 1994). The details of these spatially nonuniform regulators are becoming well characterized (Welch *et al.*, 2011), including feedback with MTs (Wittmann and Waterman-Storer, 2001). Hence, it is reasonable to ask whether similar or analogous regulatory pathways are needed to organize the spatial pattern of MT motor-based transport.

Supplemental Material can be found at:
http://www.molbiolcell.org/content/suppl/2014/06/16/mbc.E14-03-0826v1.DC1.html

In many contexts, upstream regulators of MT motor binding and activation are spatially nonuniform: posttranslational modification of tubulin is required to properly direct kinesin-1 to axons (Konishi and Setou, 2009) and modulates kinesin-3 in the yeast *Aspergillus nidulans* (Zekert and Fischer, 2009); Tau, which differentially regulates both kinesins and dynein, exhibits a concentration gradient along axons that is perturbed in disease (Dixit *et al.*, 2008). During mitosis, the kinesin-13 regulator Aurora B is active only near the kinetochore (Sanhaji *et al.*, 2010). On the other hand, spatially precise dynamics can also occur without spatially organized regulation: dendrite-specific cargo bound to dynein selects dendrites by identifying the mixed polarity of MTs (Kapitein *et al.*, 2010); complex patterns of pigment granules can result from self-organization of sliding MTs (Malikov *et al.*, 2005).

The filamentous fungus *Ustilago maydis* has been used as a model system for long-range transport of endosomes in dendrites. Unlike neurons, these fungal hyphae are easy to grow and manipulate genetically and can be readily mutated, or subjected to a variety of transport inhibitors. See Steinberg (2011) for a recent review of motor proteins and fungal morphogenesis. Early endosomes (EEs) move rapidly and bidirectionally in the cell, both toward (anterograde) and away from (retrograde) the hyphal tips. The motion and distribution of EE have been quantified experimentally (Schuster *et al.*, 2011a–c). *U. maydis* cells are ~80–100 μm long, with approximately two to four microtubules in bundles, spaced ~10 nm apart. The MT array is unipolar at cell tips and antipolar at the cell center. Only two kinds of molecular motors, kinesin-3 and dynein, mediate EE transport in this organism, although kinesin-1 is implicated in organizing dynein. Kinesin-3 attaches permanently to early endosomes, but the kinesin-EE complex binds and unbinds MT tracks. Most dynein is found closer to the cell tips in structures resembling "comets," where EEs are efficiently captured (Schuster *et al.*, 2011a). A given endosome may be bound to one dynein and four or five kinesin-3 motors at once.

A hypothesis recently proposed for EE transport in *U. maydis* (Schuster *et al.*, 2011b) suggests that EEs movement along the bulk of the filament are driven by kinesin-3. Once an EE reaches the edge zone (either tip or septum), a directional switch is driven by dynein, which carries the EE out of the edge zone, after which kinesin-3 resumes long-range transport in the opposite direction. Although this hypothesis is geometrically simple, it raises the question of what upstream mechanism controls the switches with the requisite spatial accuracy. A modified (but overlapping) hypothesis, which we explore here, is that EE transport is self-organized, with switching rates determined only by concentrations of motors and the polarity of the underlying MT array. Although our model is kinetically simpler, it is difficult to predict the consequences of this model without recourse to mathematical modeling.

Previous mathematical models also investigated the nanometer-scale interaction of motors with the lattice of individual MTs at the edge zones (Ashwin *et al.*, 2010). Experiments show that dynein molecules accumulate at the two edge zones, demonstrating that there is a capture mechanism that depends on dynactin (Schuster *et al.*, 2011a; Yeh *et al.*, 2012). Ashwin *et al.* (2010) propose that dynein capture can arise from a "traffic jam" of dynein on the MT lattice.

Here, to address questions of cell-scale organization, we derive a continuum model of EE transport in *U. maydis*. We keep the model as simple as possible while including three distinct stages of the process: MT assembly, motor organization, and EE transport. Parameters are obtained from experimental literature, and the model is validated against EE transport in mutant strains (Schuster *et al.*, 2011a–c). Our model agrees quantitatively with available data and allows us to infer behavior that is difficult to observe experimentally, such as cargo fate at MT ends within a bundle. The model also makes several experimentally testable predictions.

RESULTS

A hierarchical continuum model for microtubule arrays, motors, and early endosomes

To test whether the abundance of quantitative experimental data on *U. maydis* can be integrated into a single quantitative model, we develop a continuum, mean-field model in which transition rates are uniform in space and time, that is, depend only on local concentrations of microparticipants. The continuum modeling approach (Mogilner *et al.*, 2012) describes quantities such as motors and endosomes as densities. When used to describe discrete objects, the continuum approach is valid in three circumstances: 1) if there are many identical objects, as is the case for motors in hyphae (Lenz *et al.*, 2006), 2) when used to describe time-average behavior, or 3) as an average over an ensemble of similar systems that share basic properties. In the last two cases, the continuum approach yields densities that describe the probability of finding a molecule at a particular location. The advantage of our continuum approach is that it represents stochastic processes in a mathematically straightforward manner compared with explicit stochastic simulation (Muller *et al.* 2008; Reis *et al.*, 2012).

We build up the model in three stages, summarized in Figure 1A. First, we consider how nucleation sites determine the microtubule array structure. Second, we formulate equations for the motion and state transitions of dynein, including their transport by kinesin-1. Finally, we model the motion and state transitions of EEs. This hierarchical modeling approach ignores possible feedback between layers of the model; for example, motors have been shown to influence MT polymerization (Akhmanova and Dogterom, 2011; Hendricks *et al.*, 2012b; Pringle *et al.*, 2013). Therefore we are implicitly testing the assumption that the primary determinants of each layer are contained in the previous layer and feedbacks are of secondary importance. We also ignore feedback from downstream processes, such as dynein-dependent EE maturation (Abenza *et al.*, 2012). We summarize the model here and provide mathematical details in the Supplemental Material.

Because the features of EE transport in which we are interested appear to be approximately symmetric with respect to the tip and the septum, we refer to either side as a generic "edge zone" and differentiate them by referring to them as "left" and "right" edges.

Microtubule array with asymmetry in binding sites arises from isotropic but inhomogeneous microtubule nucleation sites

MTs in fungal hyphae are nucleated by the γ-tubulin ring complex, which is distributed throughout the hyphae, except in regions of ~10 μm from the edge zones (Schuster *et al.*, 2011b). We assume that the nucleation sites are randomly chosen to face toward left or right edges (Figure 1A). MT plus ends exhibit dynamic instability, switching between polymerization and depolymerization at known rates (Schuster *et al.*, 2011a,b). We assume that MT plus ends encountering an edge depolymerize (Seetapun and Odde, 2010). This leads to a slight variant of the model by Dogterom and Leibler (1993) and leads to a predicted mean MT length of 4.8 μm. To match the total number of MTs (Schuster *et al.*, 2011b), we estimate the nucleation rate to be ~2 MTs/s per micrometer.

Left- and right-facing MT arrays are quantitatively described by two variables: the plus-end distribution $p^R(x)$ and $p^L(x)$ and the
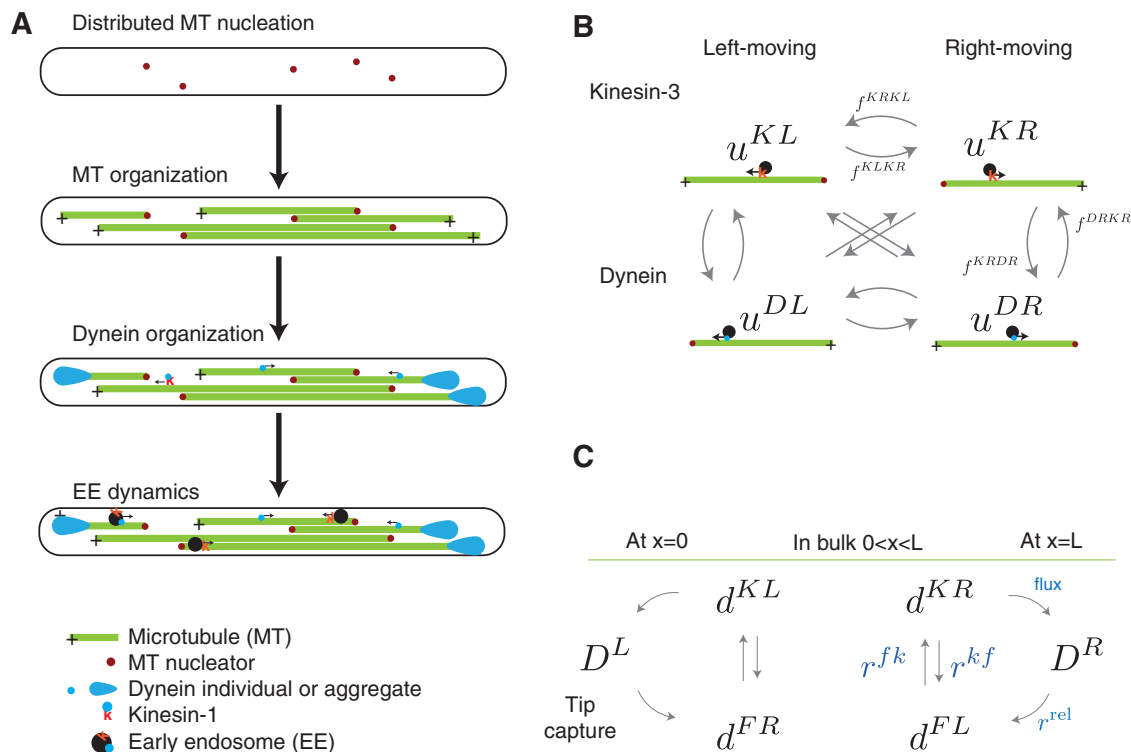
FIGURE 1: Schematic of model. (A) MT nucleation sites (red dots) spawn MTs (green rods) that grow into parallel and antiparallel arrays in fungal hyphae and neuronal axons. Dynein motors (blue) are transported to MT minus ends by intrinsic motor activity or to MT plus ends (denoted by a plus sign) by kinesin-1 (orange K's with blue dot) and accumulate in a comet-like reservoir (blue teardrops) at MT plus ends. Kinesin-3 motors (orange K's) and dynein attach to early endosomes (EE, black spheres) and walk toward MT plus and minus ends, respectively. (B) Transitions in the dynein model. In the bulk of the hyphae, away from edges, dynein is freely bound to a MT (F) or being transported by kinesin-1 (K). In the latter two cases, it can be attached to either a right-facing or left-facing MT. There are reservoirs ("tip capture") at both hyphae ends $x = 0$ and $x = L$. Individual dynein motors transition between these states, and we explore several possible sets of allowable transitions (see Figure 3B). (C) Schematic of transitions among the four EE states (u^{ij}): those bound to kinesin-3 (K) or dynein (D) moving to the left (L) or right (R). For simplicity, we assume that the hyphal tip and septum are symmetric in terms of EE and motor dynamics and therefore label these ends Left and Right. We assume that every state can switch to any other state. The rates f^{ijpq} (from state ij to state pq) are calculated based on the MT–dynein model (see Supplemental Material). Only three rates are shown in the figure for clarity. Total EE number is conserved.

density of MTs at that cross section, $N^R(x)$ and $N^L(x)$, where x describes the location along the hyphal length (Figure 2A). Note that plus-end polarity is revealed by plus-end-tracking fluorescent labels such as EB1 (Ambrose *et al.*, 2011) and Peb1 (Schuster *et al.*, 2011b), whereas polarity of MT density determines the asymmetry of binding sites on the MT lattice and is therefore the important determinant of asymmetry in MT-binding motors but is more difficult to measure experimentally. We define the array polarity in plus ends as the fraction of right-facing plus-ends,

$$p(x) = \frac{p^R(x)}{p^R(x) + p^L(x)}$$

(green dashed curve in Figure 2, D and G), and, similarly, the array polarity in MT density as

$$P(x) = \frac{N^R(x)}{N^R(x) + N^L(x)}$$

(blue solid curve in Figure 2, D and G).

To explore the importance of inhibited nucleation in the edge zones, we simulated the model assuming MTs are nucleated every-

where (Figure 2, B–D). Surprisingly, we find that these two polarity descriptors can be significantly different: whereas the array is asymmetric as observed by plus-end densities, it is symmetric in terms of MT-binding sites. We thus conclude that inhibition of nucleation in the edge zones is necessary for generating an array that is asymmetric to MT-binding molecules such as motors. Plus-end density has been measured experimentally (Schuster *et al.*, 2011b) and compares qualitatively with both Figure 2, B and E.

Dynein distribution arises from accumulation in edge zones and exhibits qualitatively different profiles depending on mechanism of interaction with kinesin-1

Dynein motors directly bound to MTs move toward the minus ends of MTs. They are also transported to MT plus ends by kinesin-1. Dynein comets accumulate in the edge zones, and the mechanism of accumulation has been described as "traffic jams" on the MT lattice (Ashwin *et al.*, 2010). Our model is agnostic with regard to the details of the mechanism of accumulation: we assume that when dynein reaches an edge, it transitions to a captured state from which it is stochastically released. Schuster *et al.* (2011a) report two subpopulations with release rates 0.1 and 0.01 s^{-1}, with about half of the
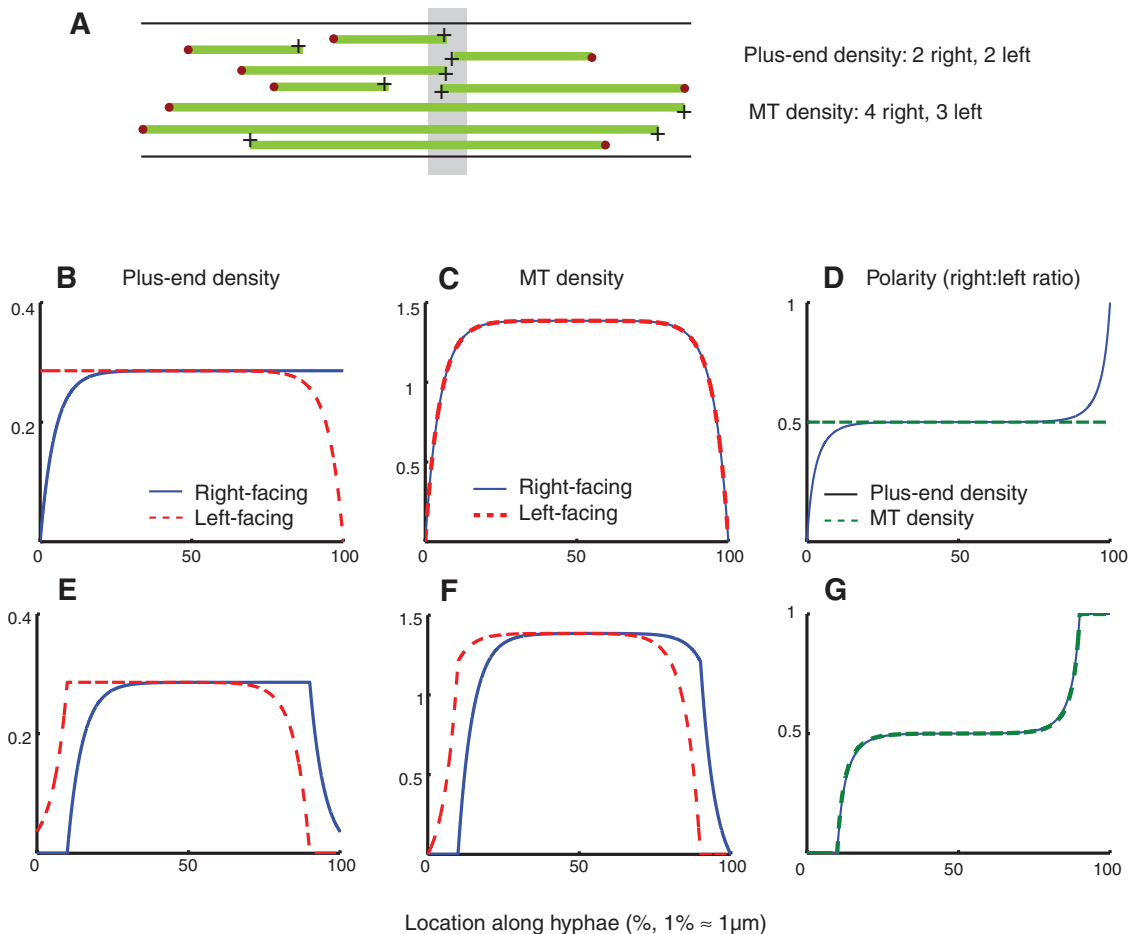
FIGURE 2: Microtubule array organization predicted by assuming isotropic nucleation that is spatially uniform (B–D) or inhibited in edge zones (E–G). (A) Local plus-end density and MT density are distinct quantities. In this schematic, the plus-end density in the shaded region is left-right symmetric. However, the local MT density (the key quantity for motor binding) in the shaded region is asymmetric. (B, E) Plus-end densities. (C, F) Microtubule densities, that is, the number of MTs traversing a cross section at this point. (D, G) The ratio of right:left MT density (green) and plus ends (blue). We refer to the ratio of MT cross-sections as the array's polarity, $P(x)$. Plus-end density has been measured experimentally (Schuster *et al.*, 2011b) and compares qualitatively with both B and E. In Supplemental Figure S1, we explore the effect of different MT length on MT array organization.

captured population corresponding to each rate. Release events from each population will contribute to the mobile population proportionally to its release rate, and therefore we can neglect the slow-release population and consider a single captive population with release rate 0.1 s^{-1}. We do not explicitly model spatial features of the edge-captured populations, and therefore effectively the model represents these populations as residing at a single point in space.

We assume total dynein amount is conserved. Recent experiment and modeling suggest that translationally active ribosomes are distributed evenly throughout hyphae (Higuchi *et al.*, 2014), raising the possibility that new dynein is created everywhere in wild-type (WT) cells. Of interest, ribosome distribution is motor dependent, potentially leading to a feedback loop between motor transport and new creation of motors that would be perturbed in dyn-ts and kin-ts mutants. Spatially distributed dynein production remains not fully characterized, and exploration of this feedback loop is beyond the scope of the present work, so we assume that dynein creation is negligible relative to dynamics of the existing population.

The biophysical details of the transition from MT-bound to kinesin-1-bound are unresolved, so we explore several possibilities, summarized in Figure 3B: i) direct switching of a dynein-kinesin-1

complex on the same MT, ii) dissociation of dynein from the MT into the cytoplasm, followed by reattachment to a MT facing either direction, by either kinesin-1 or the dynein motor domain, and iii) both pathways (i) and (ii) active, where we assume rapid rebinding of EEs once in the cytoplasmic pool. We find that all three models are capable of generating a dynein density with edge accumulation that decays away from edges. However, the dynein density in the bulk midregion varies qualitatively between models. In direct exchange (i), the density of dynein is exponentially small in the middle region. For exchange through the cytoplasm (ii), there is a basal density throughout the hyphae. When both exchange pathways are significant (iii), there can be peaks and troughs in the density profile. Quantitatively accurate measurement of the dynein density could therefore resolve which exchange mechanism is dominant. Note that Lenz *et al.* (2006) describe the density of dynein in each comet, rather than the entire spatial density profile along the hyphae.

For dynein model (i), there are two unknown parameters corresponding to the rates of switching between kinesin-1 driven and dynein driven. We can determine these parameters from the characteristic size of the regions of high dynein density (see Supplemental Material). For more complicated models (ii, iii), available
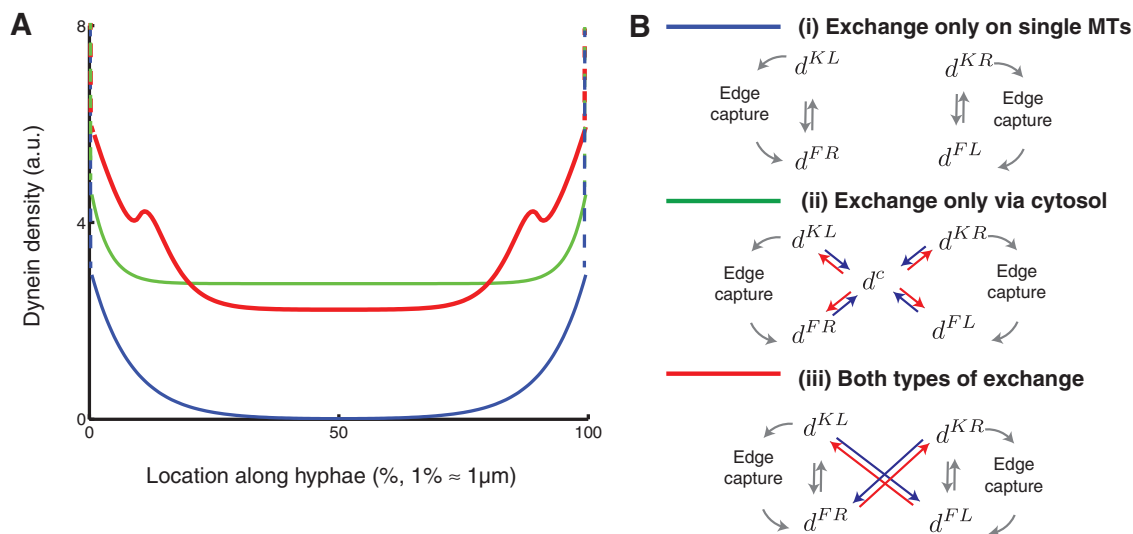
FIGURE 3: Dynein distribution (A) predicted by different models for the exchange of individual dynein molecules (B). In all three model variants, dynein reaching tips is transiently captured into a tip. The populations in these tip compartments are denoted by vertical dashed lines. In all cases, we find regions of high density near both tips (but outside the captured subpopulation) that decay exponentially moving toward the bulk. Minor features depend on whether dynein exchanges directly from minus end directed to kinesin-1 driven (i, blue curve); exchanges via a freely diffusing state in the cytoplasm (ii, green curve); or exchanges among all four possible states (iii, red curve).

experimental data are insufficient to constrain all rate constants. Therefore we are limited to concluding that these models are sufficient to produce the dynein distributions in Figure 3, without constraining parameters. However, we find qualitative differences that can be understood intuitively. In the case of direct exchange alone (i), dynein density is exponentially small near the cell middle, in contrast to the other models, which have significant density far from the edges created by exchange through the cytosol. Although this background density is not necessarily mostly cytosolic, the presence of this mode of exchange indirectly increases the dynein density. This suggests a possible experimental approach to discriminate between (i) and others. To discriminate (ii) and (iii), we observe that (iii) allows secondary features such as local maxima (see Supplemental Figure S2). These secondary features are not present in either (i) or (ii) and are due to multiple competing types of exchange, in this case through either cytoplasm or directly on a single MT.

Early endosome dynamics, validated in kinesin-3 and dynein mutants, is consistent with uniform kinetics

We next attempted to test the hypothesis that EE dynamics can result from the foregoing spatial organization of MTs and dynein with spatially uniform transition rates. The model follows experimental demonstration that an individual EE is transported either by kinesin-3 toward MT plus ends or by dynein toward MT minus ends (Schuster *et al.*, 2011b). This leads to four subpopulations of EE: those moving to the right or left, driven by either kinesin-3 or dynein. We describe these states as KR, KL, DR, and DL, where the first letter describes the driving motor and the second the direction of motion. The rate of switching to dynein-driven states is proportional to the local density of dynein, as determined by the foregoing dynein model, whereas rate of switching from left-facing MT to right-pointing MT is proportional to the MT binding-site polarity, $P(x)$, as determined by the foregoing MT array model. With this assumption, although there are 16 possible transitions between four states, there are only two unknown parameters in the EE model, representing basal transition rates onto dynein- or kinesin-3–driven states, respectively (see Supplemental Material). We fitted these

parameters to the wild-type run-length profile of EEs beginning at one edge (from Schuster *et al.*, 2011b), leading to EE densities shown in Figure 4. We report the EE density in each of the four subpopulations (Figure 4, A–D) and total EE density in steady state (Figure 4E). The total density (Figure 4E) is large everywhere along the hyphae, in agreement with observations (see, e.g., Figure 7D in Schuster *et al.*, 2011b), but is twice as large at edges compared with the cell middle. To our knowledge, large-number statistics of EE location has not been reported experimentally, and this is therefore a straightforward prediction of our model. In Figure 4, A–D, we also report the kymographs as the system approaches steady state from an initial condition with all EEs uniformly distributed and equally driven by left and right kinesin-3. From the kymographs, we find that the characteristic time scale (the time interval over which major changes take place) is ~30 s, and steady state has been effectively reached within 100 s. These time scales provide lower bounds on the time the system needs to adjust after, for example, drug treatment or temperature changes.

The same run-length distribution is shown in Figure 5, both binned into 10-μm bins (blue histogram) and as a full, continuous distribution (red curve). The continuous distribution reveals minor nonsmooth features near the boundary between edge zones, ~10 μm from either edge, approximately where MT nucleation begins. This prediction for hidden structure could be investigated experimentally by collecting data with large sample sizes and refined binning. The run-length histograms reported in Schuster *et al.* (2011b) exhibit a lack of run lengths in their shortest bin (<10 μm). This could be due to the difficulty in observing and defining such short-lived runs.

To further test our model, we simulated scenarios where either kinesin-3 or dynein was removed from the simulation, mimicking experiments with kin-ts and dyn-ts mutants in which kinesin-3 and dynein are inactive, respectively (Schuster *et al.*, 2011b). Results from simulations without dynein are shown in Figure 6, A and B. EEs accumulate in the edge zones, and their run length is increased slightly (28 μm in dyn-ts vs. 26 μm in WT), in agreement with the dyn-ts mutant. When kinesin-3 is removed from the simulation, in
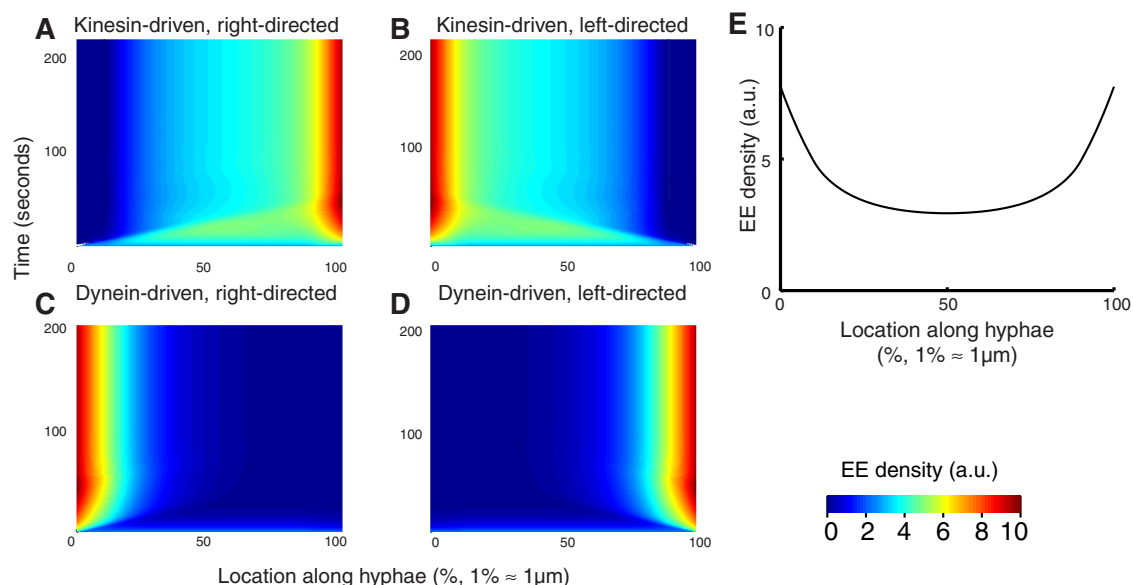
FIGURE 4: Early endosome distribution. (A–D) Kymographs (time on vertical axis, space on horizontal axis) showing four EE densities beginning from an initial state with EEs kinesin driven and spatially uniform. The steady-state distribution ($t = 500$) indicates that dynein is highly concentrated near edges, and hence is mostly responsible for EE transport here, whereas kinesin-3 has a broader distribution and hence facilitates long-range transport of EE in the bulk. (E) Steady-state distribution of EEs including all four states.

Figure 6C, EEs accumulate everywhere except for the edge regions, again agreeing with the kin-ts mutant. Taking the results together, we find that this simple model with spatially uniform switching rates is consistent with reported EE dynamics.

MT length does not significantly modulate EE dynamics

To explore the importance of our predicted mean MT length of ~5 μm, we ran simulations with a modified MT length by halving and doubling the catastrophe rate. Results for the MT array model and implications for the downstream dynein and EE models are pre-

FIGURE 5: Run lengths of anterograde early endosomes beginning from the left end. Binning the run lengths with bin size ~10 μm leads to a histogram with approximately exponentially decaying run lengths and a peak at the right end, signifying that a fraction of EEs is transported all the way to the other tip. This histogram compares well with experiment (Schuster et al., 2011b). The same simulation result shown as a continuous distribution (red) exhibits two small local features at the transition regions, corresponding to the absence of MT nucleators at the edges. Red upward-pointing arrow indicates a fraction of EEs that do not switch before reaching the right tip.

sented in Supplemental Figures S3–S5. We find the main results insensitive to these perturbations, suggesting that the size of the MT nucleation inhibition zones (10 μm) is the primary determinant of the MT array pattern. The main effect of larger MT lengths is to widen the transition region from bulk array to edge zone. We further simulated the dynein model (ii) and EE model. The effect of MT length on dynein distributions is similar to MT array organization, that is, the transitions are smoothed out. EE run lengths and distributions are minimally affected (<5% change even under twofold changes in MT length).
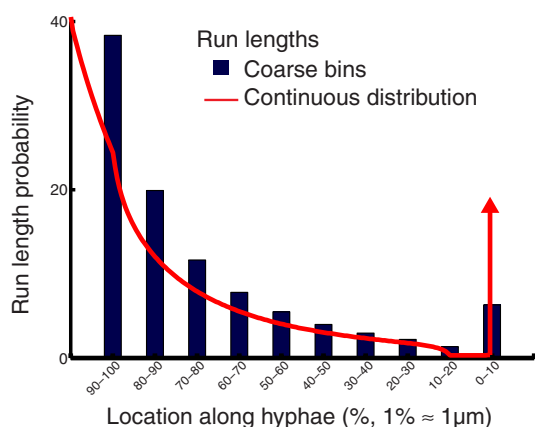
DISCUSSION

In neuronal axons, MTs form a parallel array with plus ends pointing toward the growth cone, so dynein is primarily responsible for carrying cargo in the retrograde direction (toward the soma). In dendrites, this is not the case. There, antiparallel MTs, as well as unipolar MTs, are found, mirroring the structure of the hyphae of *U. maydis*. Here we used a relatively simple set of deterministic models to represent and explore the interactions of microtubules, kinesin-3, kinesin-1, and dynein motors and their transport of early endosomes in these fungal cells. We find that much of the experimental data can be explained by such models, despite their relative simplicity. One power of a model is as a "data integrator," allowing data from different experiments to be integrated into a coherent description that highlights gaps in our understanding and possible inconsistencies. Specifically, for example, our work shows that spatial organizers of dynein are the least constrained by experiments reported in the literature. Our model also makes several testable predictions, including the EE density averaged over time (Figure 4E) and the secondary features in EE run lengths (Figure 5) that would be observed with the collection of more data and analysis of smaller bin sizes.

Mutants of dynein and kinesin-3 led to a qualitative description of EE transport (Schuster et al., 2011b) in which dynein drives short-range movement of EE away from edge zones, whereas kinesin-3 drives long-range transport across the bulk of the hyphae. This cooperation is approximately consistent with the EE transport that
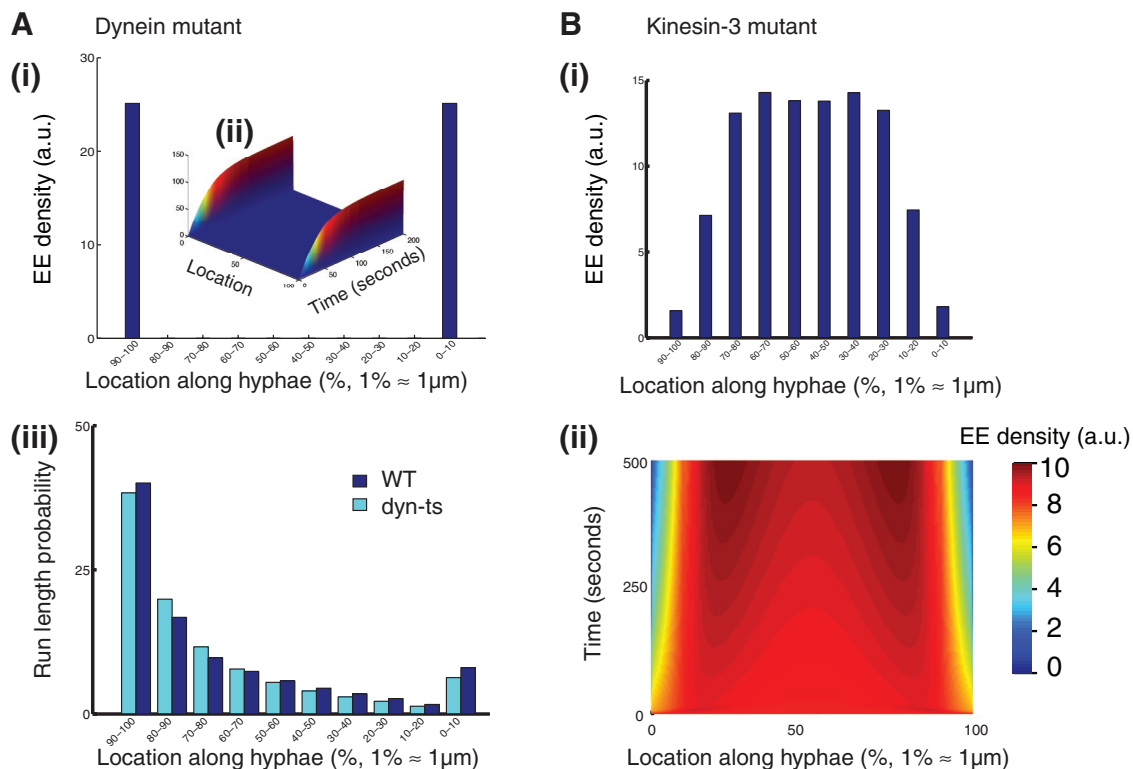
FIGURE 6: Model perturbations representing dynein and kinesin-3 mutants. (A) Model prediction for EE distribution (i, ii) and run length (iii) in dyn-ts mutants in which the activity of dynein is suppressed. The EEs accumulate at cell tips, in agreement with Schuster *et al.* (2011b). The run lengths are increased slightly compared with WT (mean run length, 27.6 μm in dyn-st and 25.6 μm in WT). (B) Model prediction of EE distribution in kin-ts mutants in which kinesin-3 is suppressed. Most EE occupy the bulk, away from the edges, with slight vacancy near the middle, in agreement with Schuster *et al.* (2011b). In both A and B, the histogram (i) shows steady-state EE distribution and (ii) shows dynamics approaching this steady state from initial conditions with uniformly distributed EEs.

arises naturally in our model. Our mathematical model clarifies this description by emphasizing that dynein and kinesin-3 are equally active everywhere, and the apparent geographical division of labor arises as a consequence of accumulation of dynein at edge zones and the details of MT array polarity, which is itself a consequence of MT nucleation inhibition in the edge zones.

Our model is deliberately agnostic about the molecular details of how an EE switches, how many motors are simultaneously active, how they are load sharing, and the effects of crowding (Conway *et al.*, 2012; Zajac *et al.*, 2013). This agnosticism allows us to focus on the larger question of how the motors are spatiotemporally regulated. Because we find that uniform switching rates are sufficient to describe experimental data, including data from mutants, in this system, the assumption that cargo switches direction through a stochastic tug-of-war would yield the same overall, cell-scale dynamics as assuming an upstream regulated switch.

One surprising result from our model of the MT array is that the array can be asymmetric in plus-end density but symmetric in MTs. Often the MT array's polarity is determined experimentally by observing plus ends (Seetapun and Odde, 2010; Ambrose *et al.*, 2011; Schuster *et al.*, 2011b). However, for motor–MT interactions, the governing quantity is polarity of MT density, that is, the number of MTs passing through that cross section, which determines the local density of binding sites. Our results demonstrate that even if the plus ends are asymmetric, the motors may experience symmetric binding and vice versa.

In many in vivo contexts, MT-motor–mediated transport occurs on bundles of MTs. An important question is thus what happens

when motor-bound cargo encounters a MT tip in the bulk of the bundle (Shubeita and Gross, 2012; Erickson *et al.*, 2013). Our model predicts a mean MT length of 4.8 μm and a mean EE run length of ~30 μm. Together, these quantities suggest that individual cargo driven toward, for example, a MT plus-end can continue traveling past the plus end onto another MT in the bundle.

The dynein densities in the edge zones exhibit dramatic comet-tail densities. To explain these, Ashwin *et al.* (2010) developed a stochastic model of individual dynein motors crowding the lattice of individual MTs. Here we demonstrated that the same comet-tail distribution can be described as the retention of dynein at the edges, combined with uniform release of dynein from the edges, followed by uniform dissociation from the MT array. Note that these models are not mutually exclusive, and, indeed, in our model, crowding may be the mechanism of dynein retention.

Similar systems-level mathematical models that consider the scale of the entire transport process, rather than individual cargo, can help elucidate other long-range bidirectional cargo transport processes. They can be extended to include MT transport (Cytrynbaum *et al.*, 2004), its role in peroxisome transport in *Drosophila* (Kulic *et al.*, 2008), and motor feedback to MT polymerization dynamics (Loughlin *et al.*, 2010). The utility of these models lies in their ability to integrate available quantitative data from many experiments into a coherent picture and show what spatiotemporal regulation, if any, is necessary. In the present case of fungal hyphae, we found that the only necessary spatial organization is inhibition of MT nucleation in the edge zones. However, we expect that modeling other systems will reveal a need for more complex upstream organization (e.g., Ikeda *et al.*,

2011). In these cases, mathematical models will provide clues to help elucidate the mechanism of upstream regulation.

MATERIALS AND METHODS

The mathematical models are described explicitly in the Supplemental Material. They consist of sets of coupled hyperbolic partial differential equations describing the time evolution of densities on a one-dimensional finite domain with no-flux boundary conditions, representing the length of the hyphae. There are 16 model parameters, 11 of which were taken from published experimental studies (Steinberg et al., 2001; Schuster et al., 2011a,b). The remaining five parameters are estimated here, each using specific experimental data as described in Results and Supplemental Material. In more complicated models of dynein transport, the number of parameters increases (Supplemental Table S1). Our results describe the model's steady state unless otherwise stated. Steady-state solutions were found analytically or numerically, using a finite-difference scheme implemented in MATLAB (MathWorks, Natick, MA).

REFERENCES

Abenza JF, Galindo A, Pinar M, Pantazopoulou A, de los Ríos V, Peñalva MA (2012). Endosomal maturation by Rab conversion in Aspergillus nidulans is coupled to dynein-mediated basipetal movement. Mol Biol Cell 23, 1889–1901.

Akhmanova A, Dogterom M (2011). Kinesins lead aging microtubules to catastrophe. Cell 147, 966–968.

Ambrose C, Allard JF, Cytrynbaum EN, Wasteneys GO (2011). A CLASP-modulated cell edge barrier mechanism drives cell-wide cortical microtubule organization in Arabidopsis. Nat Commun 2, 430–412.

Ashwin P, Lin C, Steinberg G (2010). Queueing induced by bidirectional motor motion near the end of a microtubule. Phys Rev E 82, 051907.

Bressloff P, Newby J (2013). Stochastic models of intracellular transport. Rev Mod Phys 85, 135–204.

Conway L, Wood D, Tuzel E, Ross JL (2012). Motor transport of self-assembled cargos in crowded environments. Proc Natl Acad Sci USA 109, 20814–20819.

Cytrynbaum EN, Rodionov V, Mogilner A (2004). Computational model of dynein-dependent self-organization of microtubule asters. J Cell Sci 117, 1381–1397.

Dixit R, Ross JL, Goldman YE, Holzbaur ELF (2008). Differential regulation of dynein and kinesin motor proteins by Tau. Science 319, 1086–1089.

Dogterom M, Leibler S (1993). Physical aspects of the growth and regulation of microtubule structures. Phys Rev Lett 70, 1347–1350.

Erickson RP, Gross SP, Yu CC (2013). Filament-filament switching can be regulated by separation between filaments together with cargo motor number. PLoS One 8, e54298.

Hall A (1994). Small GTP-binding proteins and the regulation of the actin cytoskeleton. Annu Rev Cell Biol 10, 31–54.

Hendricks AG, Holzbaur ELF, Goldman YE (2012a). Force measurements on cargoes in living cells reveal collective dynamics of microtubule motors. Proc Natl Acad Sci USA 109, 18447–18452.

Hendricks AG, Lazarus JE, Perlson E, Gardner MK, Odde DJ, Goldman YE, Holzbaur ELF (2012b). Dynein tethers and stabilizes dynamic microtubule plus ends. Curr Biol 22, 632–637.

Higuchi Y, Ashwin P, Roger Y, Steinberg G (2014). Early endosome motility spatially organizes polysome distribution. J Cell Biol 204, 343–357.

Ikeda K, Zhapparova O, Brodsky I, Semenova I, Tirnauer JS, Zaliapin I, Rodionov V (2011). CK1 activates minus-end-directed transport of membrane organelles along microtubules. Mol Biol Cell 22, 1321–1329.

Kapitein LC, Schlager MA, Kuijpers M, Wulf PS, van Spronsen M, MacKintosh FC, Hoogenraad CC (2010). Mixed microtubules steer dynein-driven cargo transport into dendrites. Curr Biol 20, 290–299.

Konishi Y, Setou M (2009). Tubulin tyrosination navigates the kinesin-1 motor domain to axons. Nat Neurosci 12, 559–567.

Kulic IM, Brown AEX, Kim H, Kural C, Blehm B, Selvin PR, Nelson PC, Gelfand VI (2008). The role of microtubule movement in bidirectional organelle transport. Proc Natl Acad Sci USA 105, 10011–10016.

Kunwar A et al. (2011). Mechanical stochastic tug-of-war models cannot explain bidirectional lipid-droplet transport. Proc Natl Acad Sci USA 108, 18960–18965.

Leidel C, Longoria RA, Gutierrez FM, Shubeita GT (2012). Measuring molecular motor forces in vivo: implications for tug-of-war models of bidirectional transport. Biophys J 103, 492–500.

Lenz JH, Schuchardt I, straube A, Steinberg G (2006). A dynein loading zone for retrograde endosome motility at microtubule plus-ends. EMBO J 25, 2275–2286.

Loughlin R, Heald R, Nedelec F (2010). A computational model predicts Xenopus meiotic spindle organization. J Cell Biol 191, 1239–1249.

Malikov V, Cytrynbaum EN, Kashina A, Mogilner A, Rodionov V (2005). Centering of a radial microtubule array by translocation along microtubules spontaneously nucleated in the cytoplasm. Nat Cell Biol 7, 1113–1118.

Mogilner A, Allard J, Wollman R (2012). Cell polarity: quantitative modeling as a tool in cell biology. Science 336, 175–179.

Muller MJI, Klumpp S, Lipowsky R (2008). Tug-of-war as a cooperative mechanism for bidirectional cargo transport by molecular motors. Proc Natl Acad Sci USA 105, 4609–4614.

Pringle J, Muthukumar A, Tan A, Crankshaw L, Conway L, Ross JL (2013). Microtubule organization by kinesin motors and microtubule crosslinking protein MAP65. J Phys Condens Matter 25, 374103.

Reis GF, Yang G, Szpankowski L, Weaver C, Shah SB, Robinson JT, Hays TS, Danuser G, Goldstein LSB (2012). Molecular motor function in axonal transport in vivo probed by genetic and computational analysis in Drosophila. Mol Biol Cell 23, 1700–1714.

Ridley AJ, Hall A (1992). Distinct patterns of actin organization regulated by the small GTP-binding proteins Rac and Rho. Cold Spring Harb Symp Quant Biol 57, 661–671.

Sanhaji M, Friel CT, Kreis NN, Kramer A, Martin C, Howard J, Strebhardt K, Yuan J (2010). Functional and spatial regulation of mitotic centromere-associated kinesin by cyclin-dependent kinase 1. Mol Cell Biol 30, 2594–2607.

Schuster M, Kilaru S, Ashwin P, Lin C, Severs NJ, Steinberg G (2011a). Controlled and stochastic retention concentrates dynein at microtubule ends to keep endosomes on track. EMBO J 30, 652–664.

Schuster M, Kilaru S, Fink G, Collemare J, Roger Y, Steinberg G (2011b). Kinesin-3 and dynein cooperate in long-range retrograde endosome motility along a nonuniform microtubule array. Mol Biol Cell 22, 3645–3657.

Schuster M, Lipowsky R, Assmann M-A, Lenz P, Steinberg G (2011c). Transient binding of dynein controls bidirectional long-range motility of early endosomes. Proc Natl Acad Sci USA 108, 3618–3623.

Seetapun D, Odde DJ (2010). Cell-length-dependent microtubule accumulation during polarization. Curr Biol 20, 979–988.

Shubeita GT, Gross SP (2012). Intracellular transport: relating single-molecule properties to in vivo function. In: Comprehensive Biophysics, ed. E Egelman, Waltham, MA: Elsevier, 287–297.

Soppina V, Rai AK, Ramaiya AJ, Barak P, Mallik R (2009). Tug-of-war between dissimilar teams of microtubule motors regulates transport and fission of endosomes. Proc Natl Acad Sci USA 106, 19381–19386.

Steinberg G (2011). Motors in fungal morphogenesis: cooperation versus competition. Curr Opin Microbiol 14, 660–667.

Steinberg G, Wedlich-Soldner R, Brill M, Schulz I (2001). Microtubules in the fungal pathogen Ustilago maydis are highly dynamic and determine cell polarity. J Cell Sci 114, 609–622.

Welch CM, Elliott H, Danuser G, Hahn KM (2011). Imaging the coordination of multiple signalling activities in living cells. Nat Rev Mol Cell Biol 12, 749–756.

Wittmann T, Waterman-Storer CM (2001). Cell motility: can Rho GTPases and microtubules point the way? J Cell Sci 114, 3795–3803.

Yeh T-Y, Quintyne NJ, Scipioni BR, Eckley DM, Schroer TA (2012). Dynactin's pointed-end complex is a cargo-targeting module. Mol Biol Cell 23, 3827–3837.

Zajac AL, Goldman YE, Holzbaur ELF, Ostap EM (2013). Local cytoskeletal and organelle interactions impact molecular-motor-driven early endosomal trafficking. Curr Biol 23, 1173–1180.

Zekert N, Fischer R (2009). The Aspergillus nidulans kinesin-3 UncA motor moves vesicles along a subpopulation of microtubules. Mol Biol Cell 20, 673–684.